

Deficiency of intellectual disability-related gene *Brpf1* reduced inhibitory neurotransmission in MGE-derived GABAergic interneurons

Jingli Cao,¹ Weiwei Xian,¹ Maierdan Palihati,¹ Yu Zhu,¹ Guoxiang Wang,² Yunli Xie,² Guomin Zhou,^{1,3,*} and Linya You ^{1,3,*}

¹Department of Human Anatomy & Histoembryology, School of Basic Medical Sciences, Fudan University, Shanghai 200032, China

²Institutes of Brain Sciences, Fudan University, Shanghai 200032, China

³Key Laboratory of Medical Imaging Computing and Computer Assisted Intervention of Shanghai, Fudan University, Shanghai 200032, China

*Corresponding author: gmzhou@shmu.edu.cn (G.Z.); lyyou@fudan.edu.cn (L.Y.)

Abstract

Intellectual disability is closely related to impaired GABA neurotransmission. *Brpf1* was specifically expressed in medial ganglionic eminence (MGE), a developmental niche of GABAergic interneurons, and patients with *BRPF1* mutations showed intellectual disability. To test its role in the development and function of MGE-derived GABAergic interneurons, we performed immunofluorescence staining, whole-cell patch-clamp, MGE transplantation, and mRNA-Seq to understand its effect on neuronal differentiation, dendritic morphology, electrophysiology, migration, and gene regulation, using mouse MGE-derived GABAergic interneurons infected with AAV-sh*Brpf1*. The results showed that *Brpf1* knockdown had a decreasing trend, although not significant, on the differentiation of GABAergic interneurons into parvalbumin⁺ interneurons. Moreover, increased firing threshold, decreased number of evoked action potentials, and a reduced amplitude of miniature inhibitory postsynaptic currents were observed before any significant change of MAP2⁺ dendritic morphology and *in vivo* migration ability appeared. Finally, mRNA-Seq analysis revealed that genes related to neurodevelopment and synaptic transmission such as *Map2k7* were dysregulated. Our results demonstrated a key role of *Brpf1* in inhibitory neurotransmission and related gene expression of GABAergic interneurons.

Keywords: intellectual disability; *Brpf1*; MGE-derived GABAergic interneurons; differentiation; dendritic morphology; electrophysiology; *in vivo* migration; mRNA-Seq

Introduction

Intellectual disability usually refers to a series of neurodevelopmental disorders that are obviously impaired in intelligence and adaptive function due to brain hypoplasia or organic damage (Marrus and Hall 2017; Purugganan 2018), affecting approximately 2–3% of the total population (Daily et al. 2000), with a prevalence of up to 2% in children or adolescents (Roeleveld et al. 1997; Leonard and Wen 2002). Intellectual disability not only causes a heavy burden on patients and families, but also brings a series of problems in public health, society, and education. At present, studies have shown that there are around 1396 genes related to intellectual disability (Ilyas et al. 2020), and bromodomain and PHD finger-containing protein 1 (BRPF1) is one of them. In the last few years, a total of 40 clinical cases of intellectual disability caused by *de novo* or inherited BRPF1 mutations have been reported (Mattioli et al. 2017; Yan et al. 2017; Baker et al. 2019; Pode-Shakked et al. 2019; Yan et al. 2020). Yan et al. (2017) reported that 10 patients with BRPF1 mutations had symptoms such as developmental delay, language expression disorder, and intellectual disability. Another team found 6 patients with BRPF1 mutations whose clinical manifestations were growth retardation, sagging

eyelid, and cerebellar malformations (Mattioli et al. 2017). Recent studies have further confirmed that patients with BRPF1 mutations often exhibited clinical symptoms such as intellectual disability, general developmental delay, gross motor delay, facial and ocular deformities (such as blepharoptosis and ptosis) (Baker et al. 2019; Pode-Shakked et al. 2019; Yan et al. 2020).

BRPF1 is a unique epigenetic regulatory factor, which contains two PHD fingers, one bromodomain, and one PWWP domain. BRPF1 can recognize different epigenetic markers and activate three histone acetyltransferases MOZ, MORF, and HBO1 (also known as KAT6A, KAT6B, and KAT7, respectively) (Lalonde et al. 2013; Yang 2015; Lloyd and Glass 2018). Our previous work indicated that mouse *Brpf1* plays a key role in early embryo development (You et al. 2015a), forebrain development (You et al. 2015b, 2015c), and embryonic hematopoietic stem cell maintenance (You et al. 2016). Global *Brpf1* knockout mice were lethal before E9.5 with defects such as neural tube closure, angiogenesis, and placental development (You et al. 2015a). Forebrain-specific loss of *Brpf1* led to early postnatal lethality and growth retardation (You et al. 2015c), and it has also been found that loss of *Brpf1* can regulate neuronal migration, cell cycle progression, and transcriptional control, resulting in abnormal hippocampal morphogenesis.

Received: January 08, 2021. Accepted: March 09, 2021

© The Author(s) 2021. Published by Oxford University Press on behalf of Genetics Society of America.

This is an Open Access article distributed under the terms of the Creative Commons Attribution-NonCommercial-NoDerivs licence (<http://creativecommons.org/licenses/by-nc-nd/4.0/>), which permits non-commercial reproduction and distribution of the work, in any medium, provided the original work is not altered or transformed in any way, and that the work is properly cited. For commercial re-use, please contact journals.permissions@oup.com

Another group reported that heterozygous loss of mouse *Brpf1* led to reduced dendritic complexity in both hippocampal granular cells and cortical pyramidal neurons (Su et al. 2019).

Intellectual disability is closely related to the imbalance of inhibitory/excitatory neural circuits, especially the imbalance of inhibitory circuits (Ben-Ari 2014; Nelson and Valakh 2015; Contreras et al. 2019). GABAergic interneurons are the major cellular units of the inhibitory neural circuit (Marin 2012; Ferguson and Gao 2018), and are mainly produced in the medial and caudal ganglionic eminence (MGE and CGE) and preoptic area (PoA) of the telencephalon (Xu et al. 2004; Tremblay et al. 2016). After differentiation, GABAergic interneurons migrate tangentially to the neocortex, with some of them to the cortical marginal zone (Lim et al. 2018). MGE-derived GABAergic interneurons are mainly differentiated into somatostatin (SST)⁺ and parvalbumin (PV)⁺ interneurons (Kelsom and Lu 2013; Tremblay et al. 2016), and growth number reaches a peak at E13.5 (Lim et al. 2018). GABAergic interneurons stay on the MGE for a period of time, then mostly tangentially migrate at E15.5–E16.5. Our previous work showed that mouse *Brpf1* is specifically expressed in MGE (You et al. 2014). Relatedly, the haploid mutation of *Brd1* (also called *Brpf2*) significantly reduced the number of PV⁺ interneurons in the anterior cingulate cortex of mouse (Qvist et al. 2018). We hypothesized that *Brpf1* regulates MGE-derived GABAergic interneurons and affects inhibitory neural circuits, which will eventually lead to abnormal learning, memory, and cognitive ability.

To test this, we applied mouse MGE-derived GABAergic interneurons and AAV-shBrpf1 to examine the effect of *Brpf1* deficiency on the differentiation, dendritic morphology, electrophysiological properties, migration, and gene expression of MGE-derived GABAergic interneurons by immunofluorescence staining, whole-cell patch-clamp, MGE cell transplantation, and mRNA-seq. This study will help us understand the key role of *Brpf1* on the morphology and function of GABAergic interneurons, and provide us with new insights into the pathogenesis of intellectual disability caused by BRPF1 mutations.

Materials and methods

Animals

C57BL/6 mice were used in this study and were purchased from Shanghai Slac Laboratory Animal CO., LTD. The day when vaginal plug is detected was considered to be embryonic day 0.5 (E0.5). All experimental animals were kept in an animal facility at Fudan University and all experiments were conducted in accordance with guidelines approved by Fudan University.

Primary neuron culture

Primary GABAergic interneurons were prepared from E14.5 wild-type pregnant mice. MGEs were isolated from the embryonic brains in ice-cold HBSS (Thermo, 14185052) with 1% HEPES (Thermo, 15630106) and the MGEs were transferred to a 15 ml centrifuge tube for digestion with 3 ml HBSS/HEPES containing 100 µg/ml DNase (Sigma, D4527) and 0.05% trypsin (Sigma, T8658-1vl). Centrifuge tube was transferred to a 37° water bath for 15 min and gently shaken every 3–5 min. Five milliliters Neurobasal medium (Gibco, 211030049) supplemented with 10% FBS (Gibco, 10091148), 2% B27 supplement (Gibco, 17504044), and 1% GlutaMAX-1 (Gibco, 35050061) was added to stop the digestion. The mixed liquid was centrifuged at 800 rpm for 5 min and the supernatant was removed. Neurobasal medium supplemented with 10% FBS, 2% B27 supplement, and 1% GlutaMAX-1 was added again. The neurons were then dissociated by pipetting, and the suspension was centrifuged at 1000 rpm for 5 min. Cells were then resuspended, plated at a

density of 2–5 × 10⁴ cells/well on coverslips in a 24-well plate pre-coated with poly-L-lysine (Sigma, P9155), and cultured in a neurobasal medium supplemented with 2% B27 supplement, and 1% GlutaMAX-1.

Immunofluorescence staining

Neurons were infected with AAV-scramble-GFP or AAV-shBrpf1-GFP virus at DIV3. The shBrpf1 sequence was shown in Table 1. After DIV10, GFP-expressing neurons could be gradually observed under a fluorescent microscope. At DIV14–15, immunofluorescent staining was performed to quantify the number of GABAergic interneurons that differentiated into PV⁺ or SST⁺ interneurons. Briefly, neurons were fixed in 4% paraformaldehyde (Biosharp, BL539A) in PBS (Hyclone, SH30243.01) for 20 min, permeabilized with 0.1% Triton X-100 (Sigma, X-100) in PBS for 1 h, and blocked with 10% goat serum (Proteintech, b900780) in PBS for 1 h at room temperature. Neurons were then incubated with primary antibodies at 4° overnight and second antibodies for 1 h. The primary antibodies used were mouse anti-MAP2 (1:1000, RRID: AB_2882331), rabbit anti-GFP (1:500, RRID: AB_11042881), mouse anti-GABA (1:200, RRID: AB_476667), rabbit anti-PV (1:500, RRID: AB_2880541), rabbit anti-SST (1:500, RRID: AB_2195910), and mouse anti-GFP (1:500, RRID: AB_11182611). Neurons were finally incubated with DAPI (Sigma, D9542) at

Table 1 Primer sequence

Primer name		Primer sequence
shBrpf1	Sense	GGCTTACCCTACTTGAACCT
	Antisense	AAGTTCAAGTAGCGGTAAGCC
Gapdh	F	AGGTCGGTGTGAACGGATTG
	R	TGTAGACCATGTAGTTGAGGTCA
mBrpf1	F	ATGCAGCTGACCCCTTTCCT
	R	CACTGCTGCCCTGTAGAAGA
Rnf170	F	AGAAGGAGTGAGCGACCAAGTC
	R	CTCGAAGCACTCTGACTAGCTC
Vdr	F	GCTCAAACGCTGCGTGACATT
	R	GGATGGCGATAATGTGCTGTTGC
Hrh1	F	AAGGTGACCTCTCCGACTGTCT
	R	TGGCTCAAGGTCTGGTCATTGG
Cldn19	F	GCACTCGGGTTGGAGACAGTAA
	R	GGTAGCATAACCAGGAGACAGCA
Pcdhgb1	F	CTCAGGATCTCCTGTGCGATGA
	R	GGCTTGAGAGAAACGCCAGTCA
Sec1	F	GGCGAATATGCCACGCTGTTTG
	R	CCTTTTGGCTGTGTGCGTATGC
Fgf2	F	AAGCGGCTCTACTGCAAGAACG
	R	CCTTGATAGACACAACCTCTCTC
Kctd20	F	CCACTCAAGAGAAAGAAGGCAGC
	R	TTGCTGGCTGAGAGGCATAGTC
Rcvrn	F	CTTCTCGCTCTACGACGTAGAC
	R	TCTTCTCAGCCCGCTTTTCTGG
Shroom4	F	TACAGGTTGCTGTACCGGTCCT
	R	TTGGCTTCCACTGTCCACAGG
Map2k7	F	TCAGGTGTGGAAGATGCGGTTT
	R	AAGGCAGTCATGGCTTTGAG
Asic3	F	TATGTGGCTCGGAAGTGCGGAT
	R	CAGACACAAGTGTCTTTCCGAG
Jph2	F	CAACCAGGAGTCCAACATCGCC
	R	GCTCTCAGAGTTCTCCAGGATC
Prickle4	F	AAGAAGGACCCGATCCAAGC
	R	AGGGTTTCCAGGGTGAGAGT
Ak4	F	GAAGCAGTTGCTGCCAGGCTAA
	R	GCCAGATTCTGTTAGTCTCCGTC
S1pr5	F	AGACTCTCCAACAGCTTGCAG
	R	TAGAGCTGCGATCCAAGTTGG
Nlrp6	F	CTGGCGTCATTGTGGAACCTCT
	R	TCTCACTCAGCTCCACAGAGGT

room temperature for 10 min and mounted with antifade mounting medium.

Quantification of immunofluorescent images

To study the effect of *Brpf1* knockdown on the differentiation of GABAergic interneurons, we used ImageJ Fiji (RRID: SCR_002285) software to manually count the number of GABA⁺GFP⁺, SST⁺GFP⁺, PV⁺GFP⁺ neurons and the total number of GFP⁺ neurons, the proportion of co-labeled neurons in GFP⁺ neurons was then calculated. For analysis of dendritic morphology, coverslips were observed under an inverted fluorescence microscope (Olympus) and confocal microscope (Leica SP8, RRID: SCR_018169). The images were analyzed using ImageJ Fiji. To calculate the branches and the total length of dendrites, Sholl analysis was applied. Simple Neurite Tracer plug-in was used to track the path of the neuron, and the radius was increased to cover the entire path of the neurons with the cell body as the center and a fixed value of 10 μm. The Sholl analysis plug-in was used to calculate the number of intersections between the ring and the neurite. The total length of dendrites was also displayed when tracing the path of neurites.

Electrophysiological recordings and analysis

For whole-cell patch-clamp recording, neurons were infected with a reduced titer of AAV-scramble-GFP or AAV-shBrpf1-GFP virus at DIV3 to achieve sparse labeling and the recordings were performed at DIV15. Neurons expressing GFP under high-resolution fluorescent microscope were chosen for electrophysiological recordings. Briefly, coverslips covered with neurons were transferred to a holding chamber attached to the microscope stage, containing normal-temperature artificial cerebrospinal fluid (ACSF). Electrodes with electrode solution were used to patch neurons under the fluorescent microscope. To characterize the intrinsic membrane properties of neurons, current-clamp recordings were performed and hyperpolarized and depolarized current steps were injected in 20 pA increments. The following parameters were measured to characterize the neuronal membrane characteristics: the resting membrane potential was recorded immediately after the neuronal membrane was ruptured, and the number of APs induced after different current injections were measured. The AP current threshold is defined as the first rectangular current injection that causes a spike. Offline analysis was performed using Clampfit software (RRID: SCR_011323). To study the synaptic transmission between neurons, mIPSCs were recorded. 1 μM tetrodotoxin, 10 μM NBQX, and 50 μM D-AP5 were added to ACSF. The same method to patch the neurons was applied and the data was recorded for 6 min. The amplitude and frequency were analyzed by mini-analysis software (RRID: SCR_002184).

RT-qPCR

All the following experiments were RNase-free. The total RNA was extracted by the traditional Trizol (Thermo, 15596018) method (Groppe and Morse 1993), dissolved in a suitable volume of RNase-free water, and the RNA concentration was determined using a Nanodrop (RRID: SCR_018042). The RNA was then reverse-transcribed using a reverse transcription kit (Accurate Biotechnology Co., Ltd, AG11705). The cDNA solution was subjected to RT-qPCR using TB Green Premix Ex Taq (Takara, rr420a) and prime script rt master mix (Takara, rr036a). *Gapdh* was used as the internal control, and the relative expression of the gene was calculated by 2^{-ΔΔCt} method (Livak and Schmittgen 2001). The primer sequences were shown in Table 1.

mRNA sequencing and bioinformatic analyses

The original sequencing data were analyzed using previously published methods (Trapnell et al. 2012; Pertea et al. 2016). The total RNA was extracted using Trizol method and the RNA integrity was determined using RNA Nano chip and Agilent 2100 bioanalyzer (Groppe and Morse 1993). The samples were subjected to high-throughput sequencing through the paired-end sequencing mode of the Illumina HiSeq sequencing platform (RRID: SCR_016383). For each sample, the pre-processing sequence was compared with the mouse genome sequence (release-98) by STAR software (RRID: SCR_015899) after removing the linker sequence fragments and low-quality fragments. For all samples, StringTie software (RRID: SCR_016323) was used to count the original sequence counts of known genes, and the expression of known genes was calculated using fragments per kilobase of transcript per million fragments mapped (FPKM). The DESeq2 software (RRID: SCR_015687) was used to screen the differentially expressed genes between different sample groups, and the differential expression range of log₂ (fold change) ≥ 1, log₂ (fold change) ≤ -1 and P < 0.05 was used to screen the differentially expressed genes between the two groups. The function of differentially expressed genes was analyzed by David (Huang da et al. 2009a, 2009b) website (<https://david.ncicrf.gov/>, RRID: SCR_001881), including gene ontology (GO) and kyoto encyclopedia of genes and genomes (KEGG). The raw and processed data were deposited in Gene Expression Omnibus (RRID: SCR_005012) database with GEO# GSE157903.

MGE cell transplantation and evaluation of migration behavior

MGEs from E13.5 wild-type embryonic brains were harvested and dissociated. The cell suspensions were incubated with AAV-scramble-GFP or AAV-shBrpf1-GFP for 2 h at 37°, during which the liquid was gently mixed every half hour. Each group had about 50,000 cells. The mixed liquid was centrifuged at 800 rpm for 5 min and then the supernatant was removed. The centrifugation step was repeated two to three times. The pellet was resuspended in 10 μl DMEM supplemented with 10% FBS. The cell suspension was then injected into the neocortex of wild-type P1 host. Transplanted neurons were allowed to migrate *in vivo* for 35 days before analysis. On day 35, mice were anesthetized, perfused with PBS followed by 4% PFA through the endocardium, and then the brain was carefully dissected. The brain was incubated overnight in 4% PFA, dehydrated in 30% sucrose in PBS until the sample sank to the bottom, embedded with optimum cutting temperature compound (O.C.T., Sakura, 4583), and sectioned at a thickness of 20 μm. Rabbit anti-GFP (Proteintech, 1:500) and DAPI (1:1000) were used for immunofluorescence staining. The proportion of GFP⁺ cells in each layer of the cortex was analyzed after that the stained sections were photographed by confocal microscope (Leica SP8).

Statistical analysis

Data were analyzed statistically using ImageJ Fiji and GraphPad Prism 8.0 software (RRID: SCR_002798). Differences between groups were tested by T-test. The values of P < 0.05 were considered statistically significant. *P < 0.05, **P < 0.01, and ***P < 0.001.

Data availability

Supplementary materials include Reagent Table and Supplementary Table S1. Supplementary Table S1 contains DESeq2 output and the FPKM values of genes. Gene expression data are available at GEO with the accession number: GSE157903 (<https://www.ncbi.nlm.nih.gov/geo/>).

gov/geo/query/acc.cgi?acc=GSE157903). Figures and supplementary materials had been uploaded to figshare: <https://doi.org/10.25387/g3.14215817>.

Results

Brpf1 deficiency led to a mild decreased trend on the differentiation of GABAergic interneurons into PV⁺ interneurons

To study the effect of *Brpf1* knockdown on the differentiation of MGE-derived GABAergic interneurons, we dissected mouse MGEs from E14.5 embryos for primary culture of GABAergic interneurons. Neurons were infected with AAV-scramble-GFP or AAV-shBrpf1-GFP at the 3rd day in vitro (DIV3), and immunolabeling was performed at DIV14-15. We confirmed a knockdown efficiency of approximately 40% by RT-qPCR (Figure 1D). Then the proportion of GABA⁺GFP⁺, PV⁺GFP⁺, and SST⁺GFP⁺ neurons in total GFP⁺ neurons was calculated (Figure 1). The results showed that the ratio of GABA⁺GFP⁺ neurons in total GFP⁺ neurons reached almost 100%, indicating that the majority of the cultured MGE-derived neurons were GABAergic interneurons (Figure 1, A and 1E). GABAergic interneurons are mainly differentiated into SST⁺ and PV⁺ interneurons (Kelsom and Lu 2013; Tremblay et al. 2016). Thus, we examined the ratio of PV⁺GFP⁺ or SST⁺GFP⁺ in total GFP⁺ neurons (Figure 1, B, C, F, and G), and found little effect on the differentiation of GABAergic interneurons into SST⁺ interneurons but a mild decreased trend into PV⁺ interneurons upon *Brpf1* knockdown.

Brpf1 deficiency had little effect on the dendritic morphology of MGE-derived GABAergic interneurons

The dendrites of neurons are essential for neuronal functions. Studies have shown that the complexity of neurites is closely related to some development-related diseases (Hutsler and Zhang 2010; Konopaske et al. 2014; Wang et al. 2017). To study the effect of *Brpf1* knockdown on the dendritic morphology of MGE-derived GABAergic interneurons, we dissociated E14.5 MGEs and infected primary cultured neurons with AAV-scramble-GFP or AAV-shBrpf1-GFP. Immunostaining was performed at DIV 14-15 with anti-MAP2 antibody (a specific marker for dendrites) and the quantification was calculated from 3 independent experiments (Figure 2A). Totally 33 and 37 neurons in the AAV-Scramble and AAV-shBrpf1 groups were analyzed, respectively, using Sholl analysis (O'Neill et al. 2015). The results showed that there was no significant difference in the number of intersections and total length of dendrites between the two groups (Figure 2, B and C), indicating that *Brpf1* knockdown had little effect on the dendritic morphology of MGE-derived GABAergic interneurons.

Brpf1 deficiency attenuated inhibitory neurotransmission by decreasing miniature inhibitory postsynaptic current (mIPSC) amplitude and increasing firing threshold

Patients with intellectual disability usually have reduced learning and memory abilities, delay of which is closely related to synaptic dysfunction (Volk et al. 2015; Aincy et al. 2018; Lima Caldeira et al. 2019). Synaptic dysfunction is usually determined by the characteristics of cell membranes and synaptic transmission between neurons. To assess the functional consequences of *Brpf1* knockdown on synaptic transmission, we performed whole-

cell patch-clamp to record the electrophysiological properties of MGE-derived GABAergic interneurons at DIV 15 after AAV-scramble or -shBrpf1 infection at DIV3 (Figure 3). For inhibitory neurotransmission, we measured mIPSCs. Each neuron was recorded for 6 min and the signal of the later 3 min was selected for statistical analysis (Figure 3A, a short fragment of the signal was shown). The amplitude but not the frequency of mIPSCs decreased significantly (Figure 3, B and C). For membrane characteristics, we measured resting membrane potential (RMP), action potentials (APs), and evoked APs. RMP had little change (Figure 3D). Due to few or no spontaneous APs after many trials, we recorded evoked APs. The AAV-shBrpf1 group required a larger incident current to induce the evoked APs, with a significant increase in the firing threshold (Figure 3E), although the maximum frequency of evoked APs was not affected (Figure 3F). More specifically, when the evoked APs were induced against a serial step of increasing currents, there was a significant decrease in the number of spikes at current 130, 170, and 190 pA (Figure 3G). All the results indicated that *Brpf1* knockdown attenuated inhibitory neurotransmission of MGE-derived GABAergic interneurons.

Brpf1 deficiency had little effect on GABAergic interneuron migration in vivo

Neurons after birth migrate to specific locations and form a network with surrounding cells to perform their specific functions. In order to study the localization and migration ability of MGE-derived GABAergic interneurons in the cortex upon *Brpf1* knockdown, we adopted a transplantation assay (Vogt et al. 2015; Elbert et al. 2019). Briefly, E13.5 MGE cells were infected with AAV-scramble-GFP or AAV-shBrpf1-GFP, then injected into the cortex of P1 wild-type mice by micro-syringe (Figure 4A). The transplanted cells were allowed to develop in vivo for 35 days (a time point at which mature interneuronal markers were expressed) and the proportion of GFP⁺ cells in the cortex was analyzed (Figure 4, B–D). First, we analyzed the deep (V and VI) and superficial (I–IV) layers of the cortex, and found that the proportion of GFP⁺ cells showed no significant difference upon *Brpf1* knockdown (Figure 4C). Upon further dividing cortex layers into layers I, II–IV, V, and VI, the ratio of GFP⁺ cells in each layer still had little change (Figure 4D). Thus, the mild knockdown of *Brpf1* did not affect the neuronal migration and cortical localization of MGE-derived GABAergic interneurons.

Brpf1 deficiency led to dysregulated *Map2k7* expression in MGE-derived GABAergic interneurons

To study the molecular mechanism of *Brpf1* knockdown leading to the changes in electrophysiological properties of MGE-derived GABAergic interneurons, three batches of RNA from AAV-scramble and AAV-shBrpf1 groups were extracted for mRNA-Seq analysis. The number of fragments per kilobase fragment (FPKM) of the transcript per thousand fragments was used to calculate the expression of a known gene. DESeq2 software was used to screen the differentially expressed genes (DEGs) between different groups. DEGs with $P < 0.05$ and \log_2 (fold change) ≥ 1 were considered as up-regulated genes. Similarly, DEGs with $P < 0.05$ and \log_2 (fold change) ≤ -1 were considered as down-regulated genes. 24 and 22 genes were upregulated and downregulated, respectively, upon *Brpf1* knockdown (Figure 5A and Supplementary Table S1).

GO and KEGG enrichment analysis of these genes revealed that most of the 24 up-regulated genes were involved in gene negative transcription and inflammatory response (Figure 5B and Supplementary Table S1). Among them, *Tceal7*, *Mecom*, *Vdr*, *Lrch4* were involved in negative regulation of transcription, and *Hrh1*,

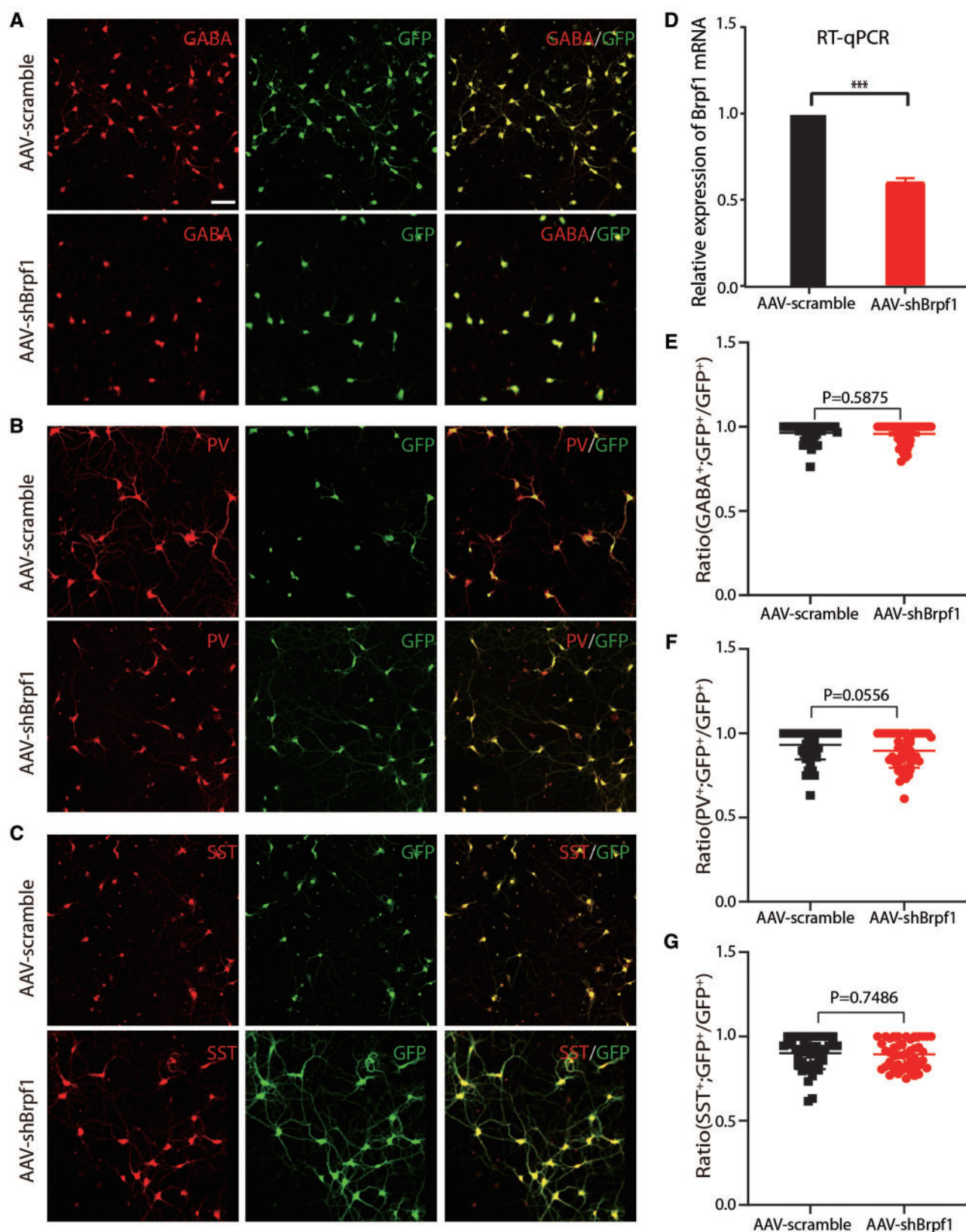


Figure 1 *Brpf1* knockdown led to a mild reduced trend on the differentiation of MGE-derived GABAergic interneurons into PV⁺ interneurons. (A–C) Representative immunofluorescent images at DIV15, which were co-labeled with GABA and GFP, PV and GFP, SST, and GFP antibodies, respectively. Scale bar, 100 μ m. (D) Quantitative mRNA analysis showed that knockdown efficiency of *Brpf1* reached approximately 40% (AAV-scramble group, $n = 5$ batches; AAV-shBrpf1 group, $n = 5$ batches; $P < 0.001$). (E–G) The ratio of GABA⁺GFP⁺, PV⁺GFP⁺, SST⁺GFP⁺ neurons in total GFP⁺ neurons upon *Brpf1* knockdown was quantified, respectively. (E) $n = 43$ and 52 fields for AAV-scramble and -shBrpf1, respectively, $P = 0.5875$; (F) $n = 55$ and 50 fields for AAV-scramble and -shBrpf1, respectively, $P = 0.0556$; (G) $n = 49$ and 45 fields for AAV-scramble and -shBrpf1, respectively, $P = 0.7486$. n was the number of fields, and the average cell count per field was about 25 neurons.

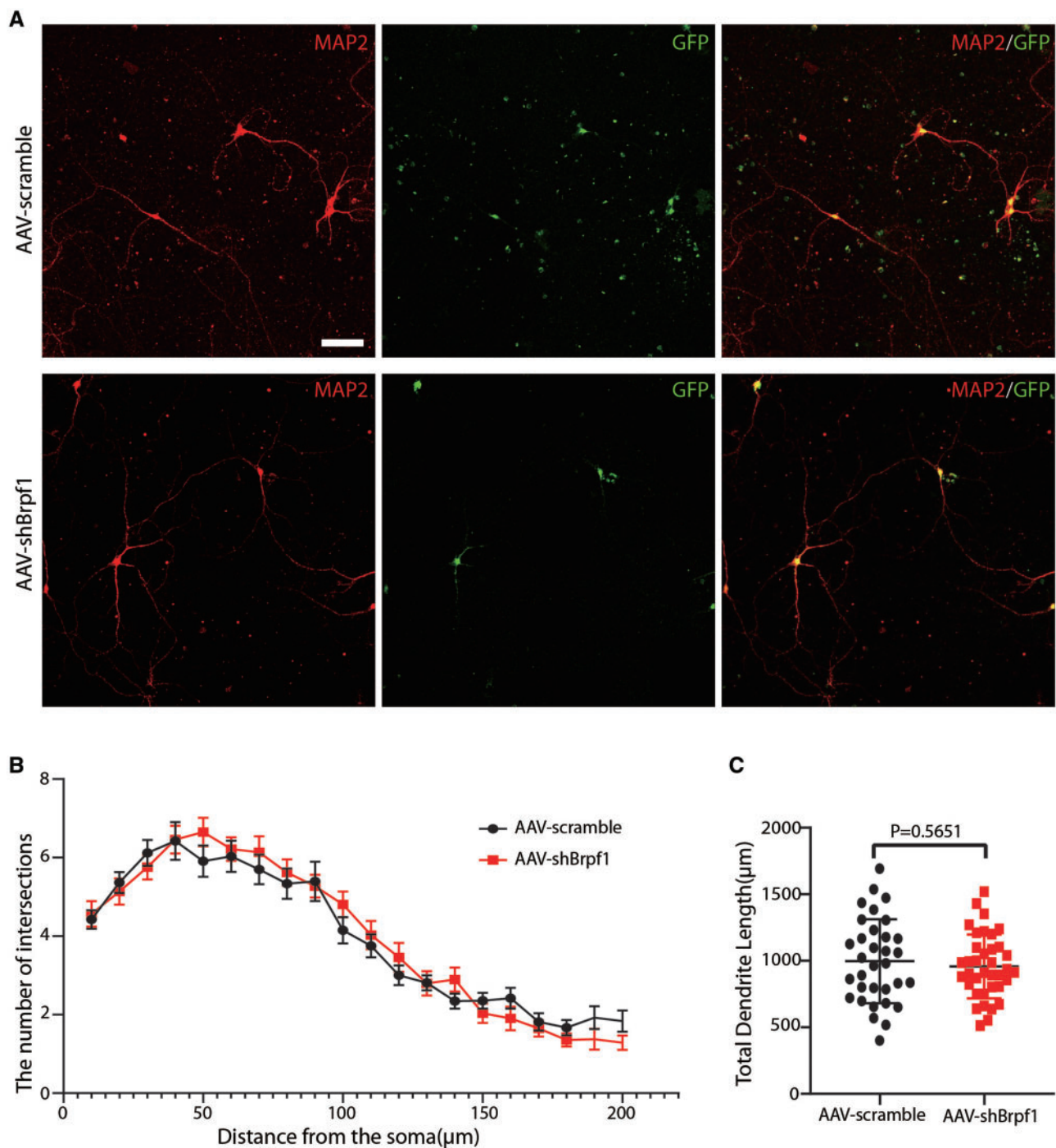


Figure 2 *Brpf1* knockdown had no significant effect on the dendritic morphology of MGE-derived GABAergic interneurons. (A) Representative immunofluorescent images of MGE-derived GABAergic interneurons immunostained with mouse anti-MAP2 and rabbit anti-GFP antibodies. Scale bar, 75 μm . (B) The mean number of intersections between dendrites and concentric circles with different radii (AAV-scramble group, $n = 33$ neurons; AAV-shBrpf1 group, $n = 37$ neurons). (C) Comparison of mean total length of neuronal dendrites (AAV-scramble group, $n = 33$ neurons; AAV-shBrpf1 group, $n = 37$ neurons; $P = 0.5651$).

Mecom, *Stab1* in inflammatory response. *Vdr* and *Hrh1* were verified by RT-qPCR (Figure 5C). However, for the 22 downregulated genes, no pathways were significantly enriched. To further explore the underlying molecular mechanism, we selected neuron-related genes among the 46 DEGs (24 plus 22) and validated by RT-qPCR (Figure 5C). For downregulated DEGs, We validated that *Map2k7* was significantly decreased upon *Brpf1* knockdown (Figure 5C). Of note, Both *Map2k7* heterozygous and tissue-specific knockout mice showed symptoms related to intellectual

disability, such as cognitive and motor dysfunction (Winchester et al. 2012; Yamasaki et al. 2017), which is similar to that of *Brpf1* knockout. This suggested that the underlying mechanism may involve dysregulated MAPK pathway via *Map2k7*.

Discussion

Accumulating clinical studies have reported totally 40 cases of patients with BRPF1 monoallelic mutations, with symptoms such

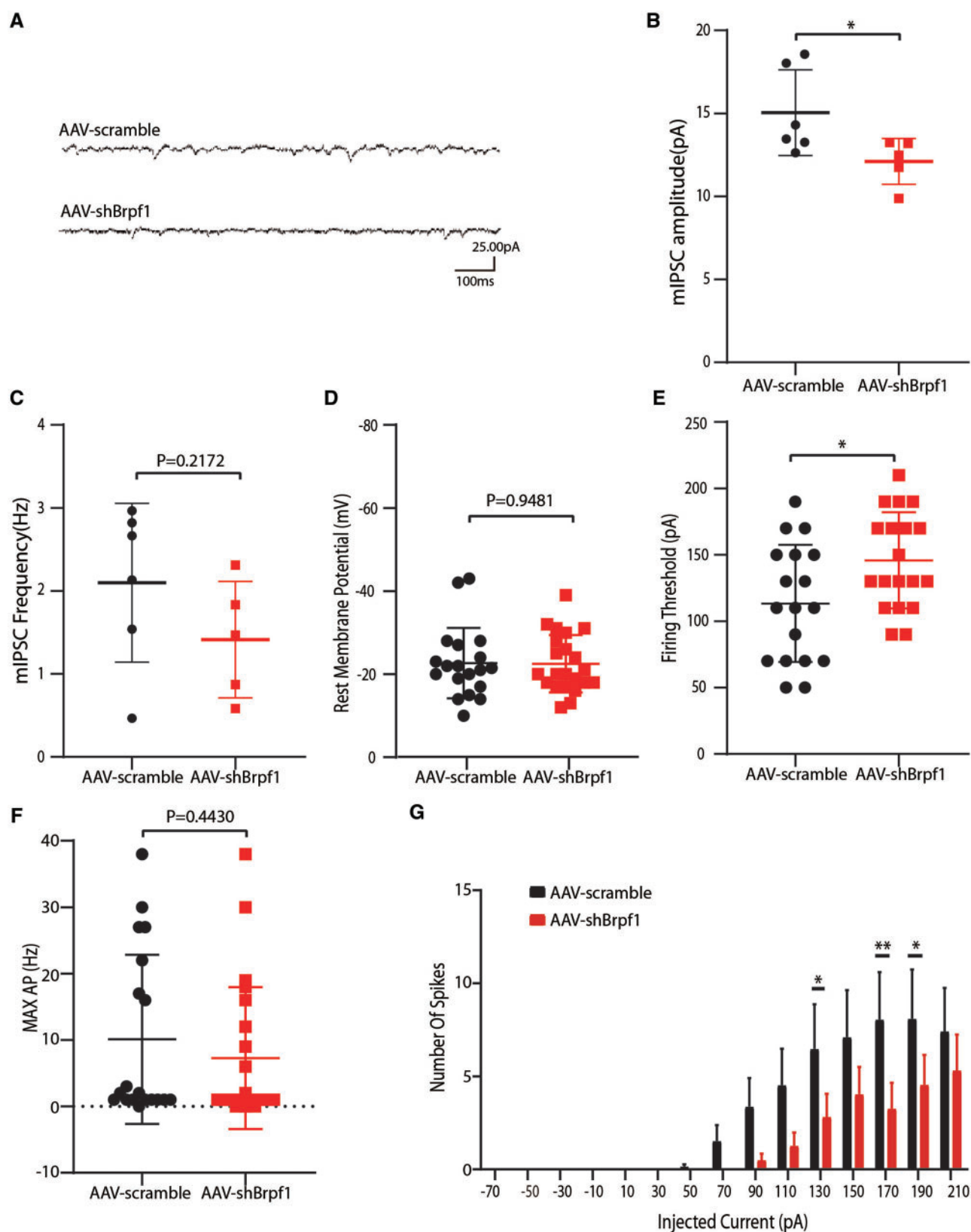


Figure 3 *Brpf1* deficiency led to attenuated inhibitory neurotransmission of MGE-derived GABAergic interneurons. (A) Representative traces of mIPSCs in GABAergic interneurons at DIV 15 between the AAV-scramble and AAV-shBrpf1 groups. 25 pA and 100 ms were shown. (B) Statistical comparison of averaged mIPSCs amplitude in GABAergic interneurons (AAV-scramble group, $n = 6$ neurons; AAV-shBrpf1 group, $n = 5$ neurons; $P = 0.0495$). (C) Statistical comparison of averaged mIPSCs frequency (AAV-scramble group, $n = 6$ neurons; AAV-shBrpf1 group, $n = 5$ neurons; $P = 0.2172$). (D) Comparable resting membrane potentials were observed (AAV-scramble group, $n = 19$ neurons; AAV-shBrpf1 group, $n = 22$ neurons; $P = 0.9481$). (E) The averaged firing threshold to induce evoked APs were compared (AAV-scramble group, $n = 19$ neurons; AAV-shBrpf1 group, $n = 22$ neurons; $P = 0.0193$). (F) The maximum frequency of evoked APs showed little change (AAV-scramble group, $n = 19$ neurons; AAV-shBrpf1 group, $n = 22$ neurons; $P = 0.4430$). (G) The number of evoked APs was induced against depolarizing current steps of increasing amplitude starting from -70 to 210 pA. (AAV-scramble group, $n = 19$ neurons; AAV-shBrpf1 group, $n = 22$ neurons; $P = 0.03972$ at 130 pA; $P = 0.0072$ at 170 pA; $P = 0.0452$ at 190 pA). * $P < 0.05$, ** $P < 0.01$.

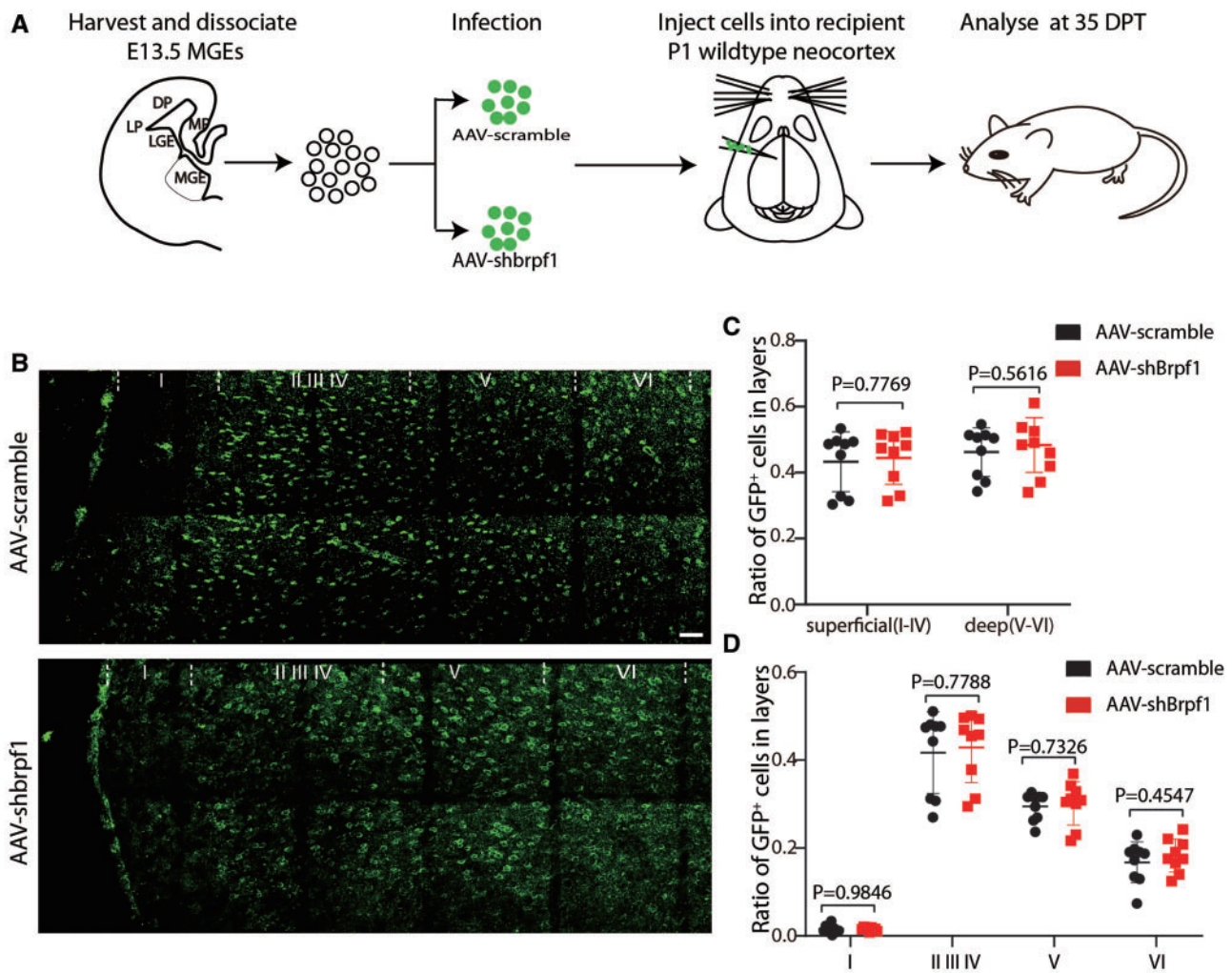


Figure 4 *Brpf1* deficiency had no effect on the neuronal migration of MGE-derived GABAergic interneurons in vivo. (A) Schematic diagram of MGE cell transplantation. In short, MGE neurons dissociated from E13.5 embryonic brains were infected with GFP-carrying adeno-associated virus (AAV-scramble-GFP or AAV-shBrpf1-GFP) and transplanted into the P1 neocortex. The proportion of GFP⁺ neurons in each cortical layer were analyzed after 35 days. (B) Representative images of GFP⁺ neurons in each layer of cortex were analyzed at day 35 after transplantation. Arrows indicated GFP⁺ neurons. Scale bar: 50 μ m. (C) Quantitative analysis of the proportion of GFP⁺ neurons in deep (V and VI) and superficial (I-IV) cortical layer, respectively (AAV-scramble, $n = 9$ mice; AAV-shBrpf1, $n = 9$ mice). (D) Quantitative analysis of the ratio of GFP⁺ neurons in layer I, II-IV, V, and VI, respectively (AAV-scramble, $n = 9$ mice; AAV-shBrpf1, $n = 9$ mice).

as intellectual disability, developmental delay, and epilepsy (Mattioli et al. 2017; Yan et al. 2017; Baker et al. 2019; Podeshakked et al. 2019; Yan et al. 2020). Impaired GABA neurotransmission is associated with mental disorders such as epilepsy and intellectual disability. Our previous work has found that *Brpf1* global knockout is embryonically lethal (You et al. 2015a), and *Brpf1* forebrain-specific knockout showed hypoplasia in hippocampus, corpus callosum, and cortex (You et al. 2015b, 2015c). Moreover, we found that *Brpf1* is specifically expressed in MGE at E14.5 (You et al. 2014), a niche where most GABAergic interneurons were born. To study monoallelic loss effect of *Brpf1*, we mildly knocked down *Brpf1* in MGE-derived GABAergic interneurons with a knockdown efficiency of about 40% (Figure 1D). Interestingly, this study found that *Brpf1* mild knockdown led to significant changes in electrophysiology (Figure 3) and a decreased differentiation trend of GABAergic interneurons into PV⁺ interneurons (Figure 1) before any overt influence in dendritic morphology (Figure 2) and neuronal migration (Figure 4). More specifically, *Brpf1* mild knockdown can sensitively cause attenuated inhibitory neurotransmission by decreasing mIPSC

amplitude and increasing firing threshold of evoked APs (Figure 3). The underlying mechanism may involve dysregulated MAPK pathway via *Map2k7*, as indicated by mRNA-Seq (Figure 5).

We found that a decreased trend of MGE-derived GABAergic interneurons to differentiate into PV⁺ interneurons upon *Brpf1* knockdown ($p = 0.056$, Figure 1). Consistently, *Brd1* (also known as *Brpf2*) heterozygous mice also displayed a decrease in the number of PV⁺ interneurons (Qvist et al. 2017, 2018). *Moz* and *Morf* were involved in regulating neurogenesis (Merson et al. 2006; Cosentino et al. 2019; Wiesel-Motiuk and Assaraf 2020). *Morf* mutant mice showed reduced ability of neural stem cells/progenitor cells differentiating into neurons, astrocytes, and oligodendrocytes, but not limited to specific neuronal types (Merson et al. 2006). Further confirmation with a more efficient knockdown/knockout in vivo will be needed to study *Brpf1*'s effect on PV⁺ interneuronal differentiation.

Dysregulation of excitatory/inhibitory neuronal circuits was closely related to various neurodevelopmental disorders (Forrest et al. 2018; Selten et al. 2018; Munoz et al. 2020) such as intellectual disability, epilepsy, and schizophrenia. Our study found that

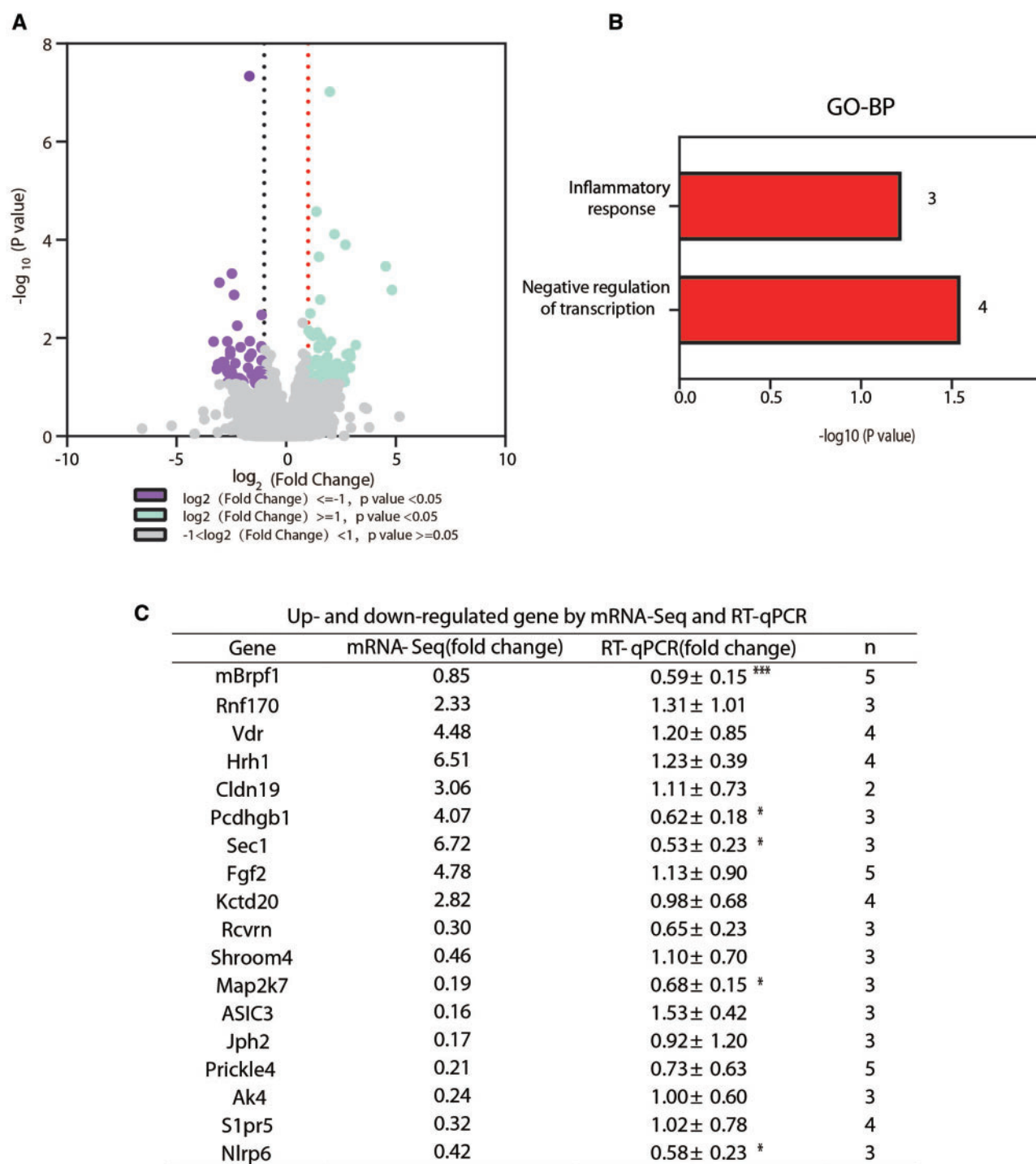


Figure 5 *Brpf1* deficiency led to decreased *Map2k7* expression in MGE-derived GABAergic interneurons revealed by mRNA-Seq. (A) Volcano plot of DEGs from mRNA-Seq, $\log_2(\text{fold change}) \leq -1$ or ≥ 1 was set as significant downregulation or upregulation (AAV-scramble group, $n = 3$; AAV-sh*Brpf1* group, $n = 3$). (B) GO-analysis of 24 upregulated and 22 downregulated genes revealed by mRNA-Seq. The number of genes involved in each Go term was indicated. (C) Validation of selected DEGs from mRNA-Seq by RT-qPCR. n indicated pairs of AAV-scramble and AAV-sh*Brpf1* groups validated by RT-qPCR. * $P < 0.05$, *** $P < 0.001$.

insufficient *Brpf1* led to abnormal synaptic transmission in MGE-derived GABAergic interneurons with reduced amplitude of mIPSCs and increased firing threshold of evoked APs, although the RMP was not altered. The RMP refers to the constant potential difference between the inside and outside of the cell membrane when the neuron is in a relatively static state. Na^+ , K^+ ion channels, and Na^+/K^+ -ATPases are the main mechanisms for maintaining the resting potential on the cell membrane. Among them,

K^+ ion channels dominate because the membrane permeability of K^+ is much higher than other ions, and the chemical gradient of K^+ is very strong (Cardozo 2016). The action potential refers to the transient and special waveform of the transmembrane potential pulse generated by the cell membrane in the resting membrane potential state by appropriate stimulation. There are two primary types of action potentials, one is generated by voltage-gated Na^+ channels, and the other is generated by voltage-gated

Ca²⁺ channels (Barnett and Larkman 2007). Studies have found that Na⁺ ion channels are closely related to inhibitory neural circuits (Catterall 2017). These may explain why *Brpf1* knockdown increased firing threshold without affecting RMP. Consistently, previous studies showed that *Brpf1* forebrain-specific (by *Emx1-Cre*) heterozygotes also had increased firing threshold of APs, reduced mEPSC frequency and amplitude in the hippocampus (Su et al. 2019). In addition, *Brd1*^{+/-} pyramidal neurons showed decreased frequency of spontaneous IPSCs and mIPSCs (Qvist et al. 2017). These results indicated that membrane properties and functional maturation of MGE-derived GABAergic interneurons were sensitive to *Brpf1* dose even with mild knockdown.

Interestingly, the mild knockdown of *Brpf1* in our study only led to significant changes in electrophysiology properties before any major influence showed in dendritic morphology and neuronal migration. Thus, we performed mRNA-Seq analysis to mainly explain the change in electrophysiology. For downregulated DEGs, *SHROOM4* was implicated in neural development associated with human X-linked intellectual disability (Hagens et al. 2006); ion transport-related genes such as *Asic3* (Wu et al. 2019), *Ak4* (Liu et al. 2009), and *Slpr5* (Tran et al. 2020) can promote the release of cations to the outside of the cell, and thus a greater current stimulation is required to induce an AP; *Map2k7* is a key gene that activates MAPK signaling (Winchester et al. 2012); NLRP6 is part of NLRP6 inflammasome and plays a crucial role in innate immunity and inflammation. *Nlrp6* could also induce apoptosis to regulate the survival of neurons (Zhang et al. 2020). For upregulated DEGs, overexpression of *Rnf170* inhibited IP3 receptor (Lu et al. 2011), which plays a key role in cell signaling; overexpression of transporter genes such as *Vdr* (Bikle 2000) and *Kctd20* (Skoblov et al. 2013) affects the assembly of some cation channels protein, and eventually leads to changes in membrane ion permeability. Our analysis revealed that *Map2k7* was significantly downregulated. Relatedly, *MOZ* knockdown led to a decrease of JNK (a key component of MAPK signaling) phosphorylation (Wiesel-Motiuk and Assaraf 2020), and patients with JNK mutations were detected with intellectual disability (Kunde et al. 2013). *MORF* disruption leads to a Noonan syndrome-like phenotype mainly via hyperactivated MAPK signaling in human and mice (Kraft et al. 2011). *Map2k7* also plays an important role in the regulation of MAPK signaling (Winchester et al. 2012). In addition, *Map2k7* heterozygous mice exhibited cognitive dysfunction (Winchester et al. 2012) and neuron-specific *Map2k7* knockout exhibited motor dysfunction such as muscle weakness and abnormal walking (Yamasaki et al. 2017). This is consistent with the learning and memory impairment in *Brpf1* mutant mice (Su et al. 2019). The mechanism of how *Brpf1* regulates *Map2k7* expression merits further investigation.

This study helps us understand the key roles of *Brpf1* in differentiation, dendritic morphology, electrophysiological characteristics, migration, and gene expression of MGE-derived GABAergic interneurons from a neurobiological level, and provides us with new insights into the pathogenesis of intellectual disability caused by *BRPF1* mutations.

Acknowledgments

We thank members from Dr. Linya You's lab for their support and help during the experiment.

Funding

This work was supported by the National Natural Science Foundation of China (81771228) to Dr. Linya You and National Natural Science Foundation of China (31571238) to Dr. Guomin Zhou.

Conflicts of interest: The authors declare no conflicts of interest.

Literature cited

- Aincy M, Meziane H, Herault Y, Humeau Y. 2018. Synaptic dysfunction in amygdala in intellectual disorder models. *Prog Neuropsychopharmacol Biol Psychiatry*. 84:392–397.
- Baker SW, Murrell JR, Nesbitt AI, Pechter KB, Balciuniene J, et al. 2019. Automated clinical exome reanalysis reveals novel diagnoses. *J Mol Diagn*. 21:38–48.
- Barnett MW, Larkman PM. 2007. The action potential. *Pract Neurol*. 7:192–197.
- Ben-Ari Y. 2014. The GABA excitatory/inhibitory developmental sequence: a personal journey. *Neuroscience*. 279:187–219.
- Bikle D. 2000. Vitamin D: production, metabolism, and mechanisms of action. In: Feingold KR, Anawalt B, Boyce A, Chrousos G, de Herder WW, Dungan K, Grossman A, Hershman JM, Hofland J, Kaltsas G et al., editors. *Endotext*. South Dartmouth (MA).
- Cardozo D. 2016. An intuitive approach to understanding the resting membrane potential. *Adv Physiol Educ*. 40:543–547.
- Catterall WA. 2017. Forty years of sodium channels: structure, function, pharmacology, and epilepsy. *Neurochem Res*. 42:2495–2504.
- Contreras A, Hines DJ, Hines RM. 2019. Molecular specialization of GABAergic synapses on the soma and axon in cortical and hippocampal circuit function and dysfunction. *Front Mol Neurosci*. 12:154.
- Cosentino MS, Oses C, Vazquez Echeagaray C, Solari C, Waisman A, et al. 2019. *Kat6b* modulates Oct4 and Nanog binding to chromatin in embryonic stem cells and is required for efficient neural differentiation. *J Mol Biol*. 431:1148–1159.
- Daily DK, Ardinger HH, Holmes GE, 2000. Identification and evaluation of mental retardation. *Am Fam Physician*. 61:1059–1067, 1070.
- Elbert A, Vogt D, Watson A, Levy M, Jiang Y, et al. 2019. CTCF governs the identity and migration of MGE-derived cortical interneurons. *J Neurosci*. 39:177–192.
- Ferguson BR, Gao WJ. 2018. PV interneurons: Critical regulators of E/I balance for prefrontal cortex-dependent behavior and psychiatric disorders. *Front Neural Circuits*. 12:37.
- Forrest MP, Parnell E, Penzes P. 2018. Dendritic structural plasticity and neuropsychiatric disease. *Nat Rev Neurosci*. 19:215–234.
- Groppe JC, Morse DE. 1993. Isolation of full-length RNA templates for reverse transcription from tissues rich in RNase and proteoglycans. *Analytical Biochemistry*. 210:337–343.
- Hagens O, Dubos A, Abidi F, Barbi G, Van Zutven L, et al. 2006. Disruptions of the novel KIAA1202 gene are associated with X-linked mental retardation. *Hum Genet*. 118:578–590.
- Huang da W, Sherman BT, Lempicki RA. 2009a. Bioinformatics enrichment tools: paths toward the comprehensive functional analysis of large gene lists. *Nucleic Acids Res*. 37:1–13.
- Huang da W, Sherman BT, Lempicki RA. 2009b. Systematic and integrative analysis of large gene lists using DAVID bioinformatics resources. *Nat Protoc*. 4:44–57.
- Hutsler JJ, Zhang H. 2010. Increased dendritic spine densities on cortical projection neurons in autism spectrum disorders. *Brain Res*. 1309:83–94.

- Ilyas M, Mir A, Efthymiou S, Houlden H. 2020. The genetics of intellectual disability: advancing technology and gene editing. *F1000Res*. 22:9.
- Kelsom C, Lu W. 2013. Development and specification of GABAergic cortical interneurons. *Cell Biosci*. 3:19.
- Konopaske GT, Lange N, Coyle JT, Benes FM. 2014. Prefrontal cortical dendritic spine pathology in schizophrenia and bipolar disorder. *JAMA Psychiatry*. 71:1323–1331.
- Kraft M, Cirstea IC, Voss AK, Thomas T, Goehring I, et al. 2011. Disruption of the histone acetyltransferase MYST4 leads to a Noonan syndrome-like phenotype and hyperactivated MAPK signaling in humans and mice. *J Clin Invest*. 121:3479–3491.
- Kunde SA, Rademacher N, Tzschach A, Wiedersberg E, Ullmann R, et al. 2013. Characterisation of *de novo* MAPK10/JNK3 truncation mutations associated with cognitive disorders in two unrelated patients. *Hum Genet*. 132:461–471.
- Lalonde ME, Avvakumov N, Glass KC, Joncas FH, Saksouk N, et al. 2013. Exchange of associated factors directs a switch in HBO1 acetyltransferase histone tail specificity. *Genes Dev*. 27:2009–2024.
- Leonard H, Wen X. 2002. The epidemiology of mental retardation: challenges and opportunities in the new millennium. *Ment Retard Dev Disabil Res Rev*. 8:117–134.
- Lim L, Mi D, Llorca A, Marin O. 2018. Development and functional diversification of cortical interneurons. *Neuron*. 100:294–313.
- Lima Caldeira G, Peca J, Carvalho AL. 2019. New insights on synaptic dysfunction in neuropsychiatric disorders. *Curr Opin Neurobiol*. 57:62–70.
- Liu R, Ström AL, Zhai J, Gal J, Bao S, et al. 2009. Enzymatically inactive adenylate kinase 4 interacts with mitochondrial ADP/ATP translocase. *Int J Biochem Cell Biol*. 41:1371–1380.
- Livak KJ, Schmittgen TD. 2001. Analysis of relative gene expression data using real-time quantitative PCR and the 2- $\Delta\Delta$ ct method. *Methods*. 25:402–408.
- Lloyd JT, Glass KC. 2018. Biological function and histone recognition of family IV bromodomain-containing proteins. *J Cell Physiol*. 233:1877–1886.
- Lu JP, Wang Y, Sliter DA, Pearce MMP, Wojcikiewicz RJH. 2011. RNF170 protein, an endoplasmic reticulum membrane ubiquitin ligase, mediates inositol 1,4,5-trisphosphate receptor ubiquitination and degradation. *Journal of Biological Chemistry*. 286:24426–24433.
- Marin O. 2012. Interneuron dysfunction in psychiatric disorders. *Nat Rev Neurosci*. 13:107–120.
- Marrus N, Hall L. 2017. Intellectual disability and language disorder. *Child Adolesc Psychiatr Clin N Am*. 26:539–554.
- Mattioli F, Schaefer E, Magee A, Mark P, Mancini GM, et al. 2017. Mutations in histone acetylase modifier BRPF1 cause an autosomal-dominant form of intellectual disability with associated ptosis. *Am J Hum Genet*. 100:105–116.
- Merson TD, Dixon MP, Collin C, Rietze RL, Bartlett PF, et al. 2006. The transcriptional coactivator Querkopf controls adult neurogenesis. *J Neurosci*. 26:11359–11370.
- Munoz MD, de la Fuente N, Sanchez-Capelo A. 2020. TGF- β /Smad3 signalling modulates GABA neurotransmission: Implications in Parkinson's disease. *IJMS*. 21:590.
- Nelson SB, Valakh V. 2015. Excitatory/inhibitory balance and circuit homeostasis in autism spectrum disorders. *Neuron*. 87:684–698.
- O'Neill KM, Akum BF, Dhawan ST, Kwon M, Langhammer CG, et al. 2015. Assessing effects on dendritic arborization using novel Sholl analyses. *Front Cell Neurosci*. 9:285.
- Perteau M, Kim D, Perteau GM, Leek JT, Salzberg SL. 2016. Transcript-level expression analysis of RNA-seq experiments with HISAT, StringTie and Ballgown. *Nat Protoc*. 11:1650–1667.
- Pode-Shakked N, Barel O, Pode-Shakked B, Eliyahu A, Singer A, et al. 2019. BRPF1-associated intellectual disability, ptosis, and facial dysmorphism in a multiplex family. *Mol Genet Genomic Med*. 7:e665.
- Purugganan O. 2018. Intellectual disabilities. *Pediatr Rev*. 39:299–309.
- Qvist P, Christensen JH, Vardya I, Rajkumar AP, Mørk A, Paternoster V, et al. 2017. The schizophrenia-associated Brd1 gene regulates behavior, neurotransmission, and expression of schizophrenia risk enriched gene sets in mice. *Biol Psychiatry*. 82:62–76.
- Qvist P, Eskildsen SF, Hansen B, Baraggi M, Ringgaard S, et al. 2018. Brain volumetric alterations accompanied with loss of striatal medium-sized spiny neurons and cortical parvalbumin expressing interneurons in Brd1 +/- mice. *Sci Rep*. 8:1–12.
- Roeleveld N, Zielhuis GA, Gabreëls F. 1997. The prevalence of mental retardation: a critical review of recent literature. *Dev Med Child Neurol*. 39:125–132.
- Selten M, van Bokhoven H, Nadif Kasri N. 2018. Inhibitory control of the excitatory/inhibitory balance in psychiatric disorders. *F1000Res*. 7:23.
- Skoblov M, Marakhonov A, Marakasova E, Guskova A, Chandhoke V, et al. 2013. Protein partners of KCTD proteins provide insights about their functional roles in cell differentiation and vertebrate development. *Bioessays*. 35:586–596.
- Su Y, Liu J, Yu B, Ba R, Zhao C. 2019. BRPF1 haploinsufficiency impairs dendritic arborization and spine formation, leading to cognitive deficits. *Front Cell Neurosci*. 13:249–249.
- Tran C, Heng B, Teo JD, Humphrey SJ, Qi Y, et al. 2020. Sphingosine 1-phosphate but not fingolimod protects neurons against excitotoxic cell death by inducing neurotrophic gene expression in astrocytes. *J Neurochem*. 153:173–188.
- Trapnell C, Roberts A, Goff L, Pertea G, Kim D, et al. 2012. Differential gene and transcript expression analysis of RNA-seq experiments with Tophat and Cufflinks. *Nat Protoc*. 7:562–578.
- Tremblay R, Lee S, Rudy B. 2016. GABAergic interneurons in the neocortex: from cellular properties to circuits. *Neuron*. 91:260–292.
- Vogt D, Wu PR, Sorrells SF, Arnold C, Alvarez-Buylla A, et al. 2015. Viral-mediated labeling and transplantation of medial ganglionic eminence (MGE) cells for *in vivo* studies. *J Vis Exp*. 52740.
- Volk L, Chiu SL, Sharma K, Hagan RL. 2015. Glutamate synapses in human cognitive disorders. *Annu Rev Neurosci*. 38:127–149.
- Wang M, Li H, Takumi T, Qiu Z, Xu X, et al. 2017. Distinct defects in spine formation or pruning in two gene duplication mouse models of autism. *Neurosci Bull*. 33:143–152.
- Wiesel-Motiuk N, Assaraf YG. 2020. The key roles of the lysine acetyltransferases KAT6A and KAT6B in physiology and pathology. *Drug Resist Update*. 53:100729.
- Winchester CL, Ohzeki H, Vouyiouklis DA, Thompson R, Penninger JM, et al. 2012. Converging evidence that sequence variations in the novel candidate gene MAP2K7 (MKK7) are functionally associated with schizophrenia. *Hum Mol Genet*. 21:4910–4921.
- Wu WL, Cheng SJ, Lin SH, Chuang YC, Huang EY, Chen CC. 2019. The effect of ASIC3 knockout on corticostriatal circuit and mouse self-grooming behavior. *Front Cell Neurosci*. 13:86.
- Xu Q, Cobos I, De La Cruz ED, Rubenstein JL, Anderson SA. 2004. Origins of cortical interneuron subtypes. *J Neurosci*. 24:2612–2622.
- Yamasaki T, Deki-Arima N, Kaneko A, Miyamura N, Iwatsuki M, et al. 2017. Age-dependent motor dysfunction due to neuron-specific disruption of stress-activated protein kinase Mkk7. *Sci Rep*. 7:7348.
- Yan K, Rousseau J, Littlejohn RO, Kiss C, Lehman A, CAUSES Study, et al. 2017. Mutations in the chromatin regulator gene BRPF1

- cause syndromic intellectual disability and deficient histone acetylation. *Am J Hum Genet.* 100:91–104.
- Yan K, Rousseau J, Machol K, Cross LA, Agre KE, et al. 2020. Deficient histone H3 propionylation by BRPF1-KAT6 complexes in neurodevelopmental disorders and cancer. *Sci Adv.* 6: eaax0021.
- Yang XJ. 2015. MOZ and MORF acetyltransferases: molecular interaction, animal development and human disease. *Biochim Biophys Acta.* 1853:1818–1826.
- You L, Chen L, Penney J, Miao D, Yang XJ. 2014. Expression atlas of the multivalent epigenetic regulator BRPF1 and its requirement for survival of mouse embryos. *Epigenetics.* 9:860–872.
- You L, Li L, Zou J, Yan K, Belle J, et al. 2016. BRPF1 is essential for development of fetal hematopoietic stem cells. *Journal of Clinical Investigation.* 126:3247–3262.
- You L, Yan K, Zou J, Zhao H, Bertos NR, et al. 2015a. The chromatin regulator BRPF1 regulates embryo development and cell proliferation. *J Biol Chem.* 290:11349–11364.
- You L, Yan K, Zou J, Zhao H, Bertos NR, et al. 2015b. The lysine acetyltransferase activator BRPF1 governs dentate gyrus development through neural stem cells and progenitors. *PLoS Genet.* 11:e1005034.
- You L, Zou J, Zhao H, Bertos NR, Park M, et al. 2015c. Deficiency of the chromatin regulator BRPF1 causes abnormal brain development. *J Biol Chem.* 290:7114–7129.
- Zhang J, Jiang N, Zhang L, Meng C, Zhao J, et al. 2020. NLRP6 expressed in astrocytes aggravates neurons injury after OGD/R through activating the inflammasome and inducing pyroptosis. *Int Immunopharmacol.* 80:106183.

Communicating editor: M. N. Arbeitman